Journal of Photochemistry and Photobiology A: Chemistry 386 (2020): 112112

DOI: https://doi.org/10.1016/j.jphotochem.2019.112112

TiO_2-REDUCED GRAPHENE OXIDE NANOCOMPOSITES: MICROSECOND CHARGE CARRIER KINETICS

A. Tolosana-Moranchel[1*], M. Faraldos[2], A. Bahamonde[2], L. Pascual[2], F. Sieland[3], J. Schneider[3], R. Dillert[3,4], D. W. Bahnemann[3,5]

[1]Departamento de Ingeniería Química, Facultad de Ciencias, C/ Francisco Tomás y Valiente 7, Universidad Autónoma de Madrid, 28049 Madrid (Spain).

[2]Instituto de Catálisis y Petroleoquímica, ICP-CSIC, C/ Marie Curie 2, 28049 Madrid (Spain).

[3]Institute of Technical Chemistry, Leibniz University Hannover, Callinstr. 5, 30167 Hannover, Germany.

[4]Laboratorium für Nano- und Quantenengineering, Gottfried Wilhelm Leibniz Universität Hannover, Schneiderberg 39, 30167 Hannover, Germany.

[5]Laboratory of Photoactive Nanocomposite Materials, Department of Photonics, Faculty of Physics, Saint-Petersburg State University, Ulianovskaia str. 3, Peterhof, Saint-Petersburg 198504, Russia.

ABSTRACT

In this work, transient absorption spectroscopy studies in the microsecond time scale were carried out to investigate the dynamics of photogenerated electron-hole pairs in TiO_2-rGO nanocomposites, prepared by a hydrothermal method, under different atmospheres: N_2, O_2, and N_2 saturated in CH_3OH. Under N_2 atmosphere, the transient absorption signal detected in the region between 450 and 700 nm dropped as the rGO mass concentration in the composite was raised. The electron transfer from TiO_2 to rGO was confirmed by using a model based on fractal surfaces which describes the decay kinetics. In the presence of methanol as hole acceptor, P25-rGO 0.5% and 1% were able to reach the maximum transient absorption faster than the other studied nanocomposites. However, after 10 μs, the P25-rGO 0.1% nanocomposite yielded the highest transient absorption signal and the best conversion and initial reaction rate in the photocatalytic degradation of dichloroacetic acid in aqueous suspensions. The effect of rGO on free electrons was investigated by detecting the transient signal at 980 nm under N_2 saturated in CH_3OH, for the different samples. It was found that the measured signals followed the same response than at 660 nm further evincing the electron transfer process. No sensitization effect of rGO was observed when the samples were excited at 450 nm.

Keywords: Transient absorption spectroscopy, TiO_2-rGO, Fractal kinetic model, Charge carrier dynamics, Reduced graphene oxide

*Corresponding authors: e-mail address: alvaro.tolosana@uam.es, schneid@iftc.uni-hannover.de

1. INTRODUCTION

Because of the increasing concern about some of the biggest challenges in the current society, such as environmental pollution and energy problems caused by the depletion of solid fuels, the development of new technologies to address these issues is necessary [1-6]. Photocatalytic treatments, an advanced oxidation process (AOPs), has been widely investigated lately because of its broad range of applications at atmospheric pressure and room temperature, which includes degradation of pollutants in water treatment [3] air pollution control [7, 8], disinfection [9-11] or water splitting for hydrogen production [12-16]. In this type of processes, a semiconductor is excited when it is irradiated by photons whose energy is equal or greater than their band-gap energy, giving rise to photogenerated electrons (e^-) and holes (h^+) that will react with adsorbed molecules located at the catalyst surface, leading to the photo-oxidation of organic matter.

Among the different semiconductors, TiO_2 has been the most investigated because of its high activity, chemical and thermal resistance, low cost and safety [3, 17]. However, TiO_2 shows some disadvantages, for example its low photonic efficiency, as most of the photogenerated electron-hole pairs recombine in the nanosecond time scale [6]. Different strategies have been carried out to improve the photocatalytic activity of TiO_2 by reducing recombination of the photogenerated charge carriers [18]. In this line, a lot of studies have been focused on the synthesis of new materials based on modifying TiO_2 by doping with metal or nonmetal elements, coupling with a semiconductor with a narrow band-gap, dye sensitization, ligand-to-metal charge transfer (LMCT) sensitization, and local surface plasmon resonance (LSPR) - sensitization techniques [19-26]. Nevertheless, nanocomposites synthesized with TiO_2 and carbonaceous structures, such as graphene, single planar sheets of sp2–bonded carbon atoms organized in benzene-ring structure, have been reported to be a good solution to achieve this goal because of the excellent properties of graphene including a large surface area, good electrical and thermal conductivity [1, 11, 27]. However, due to the lack of functional groups of non-functionalized graphene, the direct synthesis of graphene-based TiO_2 materials cannot be carried out [28]. As a result, the synthesis of these nanocomposites can be well performed by using graphene oxide (GO) which is further treated to obtain reduced graphene oxide (rGO) [11, 17, 29]. Several research articles have reported higher photocatalytic activity and faster reaction rates when GO/rGO-modified TiO_2 photocatalysts were used for organic pollutant photodegradation, dye photoremoval, bacterial inactivation and H_2 production [30-34]. Depending on the reduction degree of GO the valence band and conduction band position are shifted, which means that when oxygen content in GO is high enough GO could even act as a photocatalyst or a photosensitizer [35, 36]. Therefore, it is crucial to know the role played by rGO in TiO_2-graphene nanocomposites since depending on the bands position and the excitation wavelength, the photocatalytic process can take place by different mechanisms, for example, electrons could be transferred from TiO_2 to rGO or vice versa [28].

In this context, transient absorption spectroscopy (TAS) is a time resolved technique useful to determine the formation, trapping and recombination dynamics of the photogenerated electrons and holes. In TAS experiments, charge carriers can be quantitatively detected in different time scales subsequently to exciting the sample by a laser pulse. The change of reflectance or transmittance after employing a flash lamp allows monitoring the kinetics of the different processes [6, 37]. The advantage of studying the charge carrier dynamics of nanopowders is that TiO_2 suspensions stability problems can be avoided and the transient signal can be measured in the near-IR and IR wavelength range as the optical absorption of solvents is minimized [38]. Besides, the obtained results can be correlated with the photocatalytic performance [37].

Only one previous study focused on charge carrier kinetics in TiO_2-rGO nanocomposites have been reported in the literature [39]. However, in this study a TiO_2-rGO films were synthesized by a different method and deposited on FTO substrates which means different morphologies and properties of the nanocomposites. Moreover, the time domain of the transient absorption measurements performed in this study was broad and no detailed explanation of the transfer, trapping and recombination processes of the electron/hole pairs was given. Other works have reported charge carrier kinetics of modified photocatalysts with rGO, but visible excitation wavelengths or composites more complex than rGO-TiO_2 were used for different applications, such as H_2 production [40]. Thus, in this work, transient absorption spectroscopy in the microsecond time scale was applied to study thoroughly the dynamics of photogenerated electron-hole pairs in UV light excited TiO_2-rGO nanocomposites, synthesized through a hydrothermal treatment. The role played by rGO was studied by monitoring the kinetics of trapped holes/electrons and free electrons of nanocomposites with different rGO mass doping ratios, when they were excited at 355 nm. Runs were carried out under different atmospheres to examine the influence of electron and hole scavengers. Furthermore, in order to determine whether rGO acts as a photosensitizer, all these studied nanocomposites were also excited at 450 nm. The charge carrier signals were analyzed in detail by fitting the experimental data to a model based on fractal surfaces. Evidences of electron transfer from TiO_2 to rGO in the nanosecond scale were found. However, no sensitization effect was detected when the nanocomposite was excited with 455 nm radiation despite the fact that the TiO_2-rGO absorbs visible light. Finally, the photocatalytic activity was tested carrying out photodegradation runs of dichloroacetic acid in aqueous suspensions. This compound was selected because of his presence owing to the biological degradation of chlorinated hydrocarbons [41].

2. EXPERIMENTAL SECTION

2.1 Materials

Graphene oxide (GO) water suspension (0.4 wt% concentration) was purchased from Graphenea Company. Titanium dioxide P25 Aeroxide® (80:20 anatase-rutile, BET specific surface area 54

$m^2 \cdot g^{-1}$, average anatase and rutile crystal size of 21 and 33 nm respectively) was provided by Evonik Company.

Deionized water (H_2O) was supplied by a Millipore Milli-Q system with a resistivity equal to 18.2 MΩ·cm. Dichloroacetic acid (DCA, ≥99%) was purchased from Sigma-Aldrich, methanol was analytical grade and all the chemicals were used as received without further purification.

2.2 Synthesis of P25-rGO

P25-rGO composites were prepared by a hydrothermal method. Briefly, 2 g of TiO_2 P25 were suspended in 400 mL of deionized water and dispersed for 1 hour using a 100 MHz tip (Misonix Microson 2000XL). Subsequently, the desired amount of GO was added to the suspension and sonicated for another hour to achieve a good dispersion of GO sheets and a homogenous medium. After sonication, the mixture was transferred to a 600-mL Teflon-lined stainless steel autoclave reactor and underwent hydrothermal treatment for 18 h at 120 ºC. After that the composite was collected by centrifugation and dried in air at 60 ºC overnight. The weight ratio GO:P25 used in the synthesis was 0, 0.1, 0.5 and 1% and the photocatalysts were denominated as P25-rGO 0%, P25-rGO 0.1%, P25-rGO 0.5% and P25-rGO 1% respectively.

2.3 Photocatalysts Characterization

Diffuse reflectance spectra were recorded with a UV-Visible Agilent-Varian, Cary 5000, equipped with an integrating sphere. Analyses of the band gap transitions of the samples were made using the equation $(\alpha \cdot h \cdot v)^{1/2} = A \cdot (hv - Eg)$ [42]. A Renishaw Micro Raman spectrometer (λ = 532 nm) equipped with a 20 mW He-Ne laser emitting at 532 nm was used to obtain the Raman spectrum of the powders. The spectra were recorded using 5 repetitions, 10 seconds of acquisition time and 0.2 mW of incident power.

Energy Dispersive X-Ray Analysis (EDX) was performed on a Hitachi S-3000N electron microscope equipped with Oxford Instruments INCAx-sight. Crystal structure of the photocatalysts were analysed with a X-ray polycrystal PANalytical X´Pert PRO using nickel-filtered Cu Kα (1.541874 Å) radiation operating at 40 kV and 40 mA, with a 0.02° step size and accumulating a total of 50 s per point. Crystallite sizes were estimated by employing the Scherrer equation [43] and the crystalline phases were identified by comparing with ICDD PDF database [44]. Transmission Electron Microscope (TEM) study of the composites was carried out in a field emission gun JEOL 2100F microscope operating at 200 KV. Specimens for TEM were prepared by dry deposition of the composites in a lacey carbon copper grid. The specific surface areas were determined by the Brunauer-Emmett-Teller (BET) method [45] based on N_2 isotherm data measured at 77 K in a Micromeritics ASAP 2420 apparatus on samples previously outgassed overnight at 413 K to a vacuum of $<10^{-4}$ Pa to ensure a dry and clean surface.

Transient absorption spectroscopy (TAS), described previously in more detail [46], was carried out using an Applied Photophysics LKS 80 Laser Flash Photolysis Spectrometer. The proper diffuse reflectance accessory was used to measure in diffuse reflectance mode. A Nd-YAG laser

(Quantel; Brilliant B; 3rd harmonic, 355 nm) was used to excite the samples. A module with optical parametric oscillator technology (OPOTEK MagicPRISM) was set up to tune the laser wavelength when the samples were excited at 450 nm. Samples were light up by a pulsed xenon lamp (Osram XBO; 150 W) to analyze light absorption of the photogenerated transient species. Afterwards, the diffusely reflected light was led to the monochromator and detector (Hamamatsu PMT R928). The photometric light level was kept high for analyzing the photocatalysts. In those experiments in which the absorption of the transient species was measured at 980nm, an infrared laser diode (Roithner Lasertechnik, RLCO-980-1000-F) with an output power of 1 W was used as analyzing light to achieve a high light level. When the samples were excited at 450 nm a 475 nm longpass filter were employed between the lamp and sample to prevent the sample to be excited by UV irradiation of the probe light.

For all the experiments excitation energy densities of 2.2 $mJ \cdot cm^{-2}$ per pulse were used, monitored by a Maestro energy meter (Gentec-EO). A 100 Ω value was always used as terminal resistance and the number of averages was 12 shots. Regardless of the experiment, data were acquired for 90 μs after the laser pulse.

All the samples were powder placed into a quartz flat cuvette and they were flushed with nitrogen gas, oxygen gas or nitrogen gas saturated in methanol for more than 30 minutes before performing the measurements.

To analyze the results obtained by the diffusely reflected light, the optical reflectance changes ΔJ of the samples were calculated from the absorbance values calculated by means of the software of the instrument.

$$\Delta J = 1 - 10^{-Abs} = \frac{I_0 - I}{I_0} \qquad (1)$$

Where ΔJ can be correlated with the transient absorption of the photogenerated species and I_0 and I are the reflected light before and after the laser pulse, respectively.

2.4 Photocatalytic activity

Photodegradation runs were carried out in a stirred 1 L Pyrex slurry photoreactor at atmospheric pressure and room temperature [47]. The photoreactor was surrounded by 6 UV-A lamps and 4 day-light lamps of 15 W each. Dichloroacetic acid (DCA) photo-oxidation runs were carried out suspending 250 $mg \cdot L^{-1}$ of the desired photocatalyst in a 2 mM DCA solution. The reaction was performed at natural pH (near 2.5) with oxygen being continuously bubbled (flow of 75 $Ncm^3 min^{-1}$). Firstly, the reactant mixture was stirred in dark conditions during 30 min to guarantee homogeneous mixing and take into consideration the adsorption equilibrium stage.

DCA and Cl^- concentrations were measured by Ion Chromatography with chemical suppression (Metrohm 883 IC) and a conductivity sensor using a Metrosep A supp 7-250 column (250mm

length, 4 mm diameter) as stationary phase. Total organic carbon (TOC) was measured by an infrared detector TOC-VCSH/CSN Shimadzu analyzer.

3. RESULTS AND DISCUSSION

3.1 Photocatalyst characterization

In order to study the morphology, structure and composition of the nanocomposites, several characterization techniques were used. Some physico-chemical properties are summarized in Table 1.

Bare TiO_2 showed a BET surface area (S_{BET}) near 57 $m^2 \cdot g^{-1}$. After the junction of rGO no significant modifications in the surface area values were observed and ~60 $m^2 \cdot g^{-1}$ was obtained for all the TiO_2-rGO photocatalysts. XRD measurements revealed that P25-rGO 0% consisted of a mixture of anatase (~81%) and rutile, (~19%). No phase transition was detected in the TiO_2 after being modified with rGO and the crystal sizes of both crystalline phases remained almost unchanged. It is noteworthy that no characteristic diffraction peaks for rGO or GO species were detected, probably on account of the low amount of GO added [48]. The optical band gap energy of the nanocomposites was determined through the Tauc plots. However, after the modification of TiO_2 with rGO, the band gap values were similar to the obtained for bare TiO_2, which indicates that new energy levels were not formed in the band gap.

To verify the presence of carbon species in the nanocomposites and study the crystal structure of the TiO_2-rGO nanomaterials, Raman spectroscopy was employed. The Raman spectra of GO, P25-rGO 0%, P25-rGO 0.1%, P25-rGO 0.5% and P25-rGO 1% are plotted in the Supplementary Information Figure S1 (every spectrum was normalized to the 1340 cm^{-1} peak). The four characteristic peaks for anatase (inset of Figure S1) were detected at 142 cm^{-1}, 392 cm^{-1}, 511 cm^{-1}, and 634 cm^{-1} in all samples spectra. Regarding GO, the D and G bands were observed at 1340 and 1605 cm^{-1} respectively. The D band was ascribed to disordered graphitic carbon because of the defects created by the presence of oxygen functional groups. On the other hand, the G band was attributed to the ordered graphitic carbon [11, 48, 49]. These characteristic peaks were also identified in the spectra of the TiO_2-rGO nanocomposites. It could be noted that the higher the amount of rGO added, the higher the signal of the D and G peaks compared to the representative peaks of anatase. The area of the D and G band was calculated and the ratio A_D/ A_G (shown in Table 1) was compared for the different samples. While GO yielded an A_D/ A_G value close to 1.13, indicating a disordered structure [17, 50], values around 1.4 were estimated for P25-rGO 0.1%, P25-rGO 0.5%, and P25-rGO 1%. The increase of the ratio A_D/ A_G is the result of the strong interaction between TiO_2 and rGO sheets, giving rise to a higher disorder degree as a consequence of the reduction of GO and the contribution of remaining oxygenated functional groups [17, 19, 39, 51]. EDX analysis of the photocatalysts were performed and data are shown

in Table 2. These data further confirmed the presence of rGO in the nanocomposite as the carbon content rises on increasing the rGO/TiO_2 ratio.

Samples have been observed by TEM to study structural aspects. Figure 1(a) shows a representative micrograph of the photocatalyst without graphene oxide. The particles of TiO_2 had a size between 10 and 30 nm and some aggregates were formed. The inset shows the SAED (Selected Area Electron Diffraction) pattern of the aggregate, in which diffraction rings corresponding to both phases (anatase and rutile) were indistinguishable due to the proximity of their interplanar distances. Figure 1(b) shows an HRTEM micrograph of the TiO_2 particles. Most of the analyzed particles showed the anatase structure, in good agreement with the results obtained by XRD. One of these particles oriented in [111] has been indexed in the figure. As the rGO was incorporated into the composite, its presence became increasingly evident, being in the case of the P25-rGO 0.1% sample, in fact, difficult to find. Fig 1(c) and Figure 1(d) display HRTEM micrographs of the P25-rGO 0.1% and P25-rGO 0.5%, respectively. Both micrographs show how some particles were coated, at least partially, by rGO sheets. In the image of 0.5 wt.%, the rGO sheet could be also seen over the particles (yellow arrow), indicating that the sheet was folded over them. A more detailed study was carried out with P25-rGO 1%, in which the possibilities of seeing the rGO sheets were greater. Figure 1(e) shows a TEM image showing a big sheet of rGO covered by TiO_2 particles. The sheet can be easily seen at the borders of the aggregate (marked with red arrows). A more detailed HRTEM area is shown in Figure 1(f). In the high resolution image it can be observed that the sheet seems to wrap up several particles, which are marked in the image with red arrows. Therefore, the sheet puts these particles in contact with each other leading to an intimate contact between them and thus providing a good path for the electron transfer from the photo-excited TiO_2 to rGO.

3.2 Study of charge carriers in TiO_2 and TiO_2-rGO nanocomposites

Many studies have been reported showing the enhanced photocatalytic activity of TiO_2 nanocomposites when they were combined with reduced graphene oxide (rGO) [11, 29, 49, 50, 52, 53]. In order to achieve a better understanding of the effect of reduced graphene oxide on the photocatalytic activity, transient absorption experiments in the microsecond domain were performed using TiO_2 and TiO_2-rGO powders with rGO relative mass concentration of 0.1, 0.5 and 1%. Nanocomposites were excited with laser pulses of light with a wavelength of 355 nm and the energy of the laser was 2.2 $mJ \cdot cm^{-2}$ per pulse.

In this study, the signal at 400 nm will be used to follow the decay kinetics of trapped holes, in good agreement with other reported results [54-57]. Nevertheless, it has been reported that the type of trapped holes which exhibits transient absorption in this range corresponds to deeply trapped holes which turn out to be unreactive [6, 58]. The 660 nm signal was assigned to trapped electrons since previous reports associated a maximum around 650 nm with trapped electrons.[6,

58] Further studies revealed that free electrons dispersed in the bulk showed transient absorption in the IR range [6, 57].

Transient absorption spectra, at various times after laser excitation, under N_2 atmosphere are shown in Figure 2. Broad and featureless spectra were immediately observed after the laser pulse as a consequence of the overlap of the photogenerated electrons and holes.[54, 59] Since photogenerated charge carriers are known to be trapped or recombined at the femto/pico-second and nanosecond scale, the transient absorption can be ascribed to trapped electrons and holes in trapping sites such as Ti^{3+} $O^{-\bullet}$ or $OH^{\bullet}$ [6, 54, 56, 60]. This is well supported by the fact that the spectral shape did not change at the time scale measured.

By comparing the studied TiO_2-rGO nanocomposites spectra (Figure 2) a noteworthy decrease of the initial transient absorption intensity is observed. Several interpretations for the observed differences between bare TiO_2 and TiO_2-rGO may be considered. First, the most direct explanation is that the photogenerated electrons in the CB of TiO_2 are transferred to the reduced graphene oxide surface, likely in the picosecond time domain as was observed in water oxidation using α-Fe_2O_3/rGO photocatalysts.[61] Once transferred to the rGO surface, the electrons can undergo ultrafast relaxation processes, in 2.5 picoseconds after excitation, or be trapped by the oxygenated functional groups that remain in the rGO structure after hundreds of picoseconds [51, 62, 63]. Nevertheless, this electron transfer could not be observed in our experiments since the first measured point was taken at 0.3 μs after the laser excitation. Actually, similar electron transfer process was reported at short period of times, between 1.4 and 3.2 ps [64].

A second interpretation could be related to the ground state absorption of P25-rGO nanocomposites. The Kubelka-Munk function, α/S where α and S are the absorption and scattering coefficients respectively, is depicted in the 300-800 nm range in the Supplementary Information Figure S2. The evaluated absorption spectra at the excitation wavelength were very similar in all cases. However, in the visible region the absorption increases nearly proportionally to the rGO content whereas bare TiO_2 showed negligible absorption above 400 nm. A higher ground absorption state causes a reduction of the transient absorption intensity because of a decrease of the path length, and therefore of the amount of scattered probe light [64]. The higher the rGO content, the higher the light-block effect, being the light absorbed by TiO_2 compromised and the charge generation reduced [39]. However, it is worth mentioning that when the transient absorption spectra of P25-rGO 0.5% and 1% (Figure 2) nanocomposites are compared, no further reduction of the intensity is observed, even though the ground state absorption for P25-rGO 1% was higher than that for P25-rGO 0.5% nanocatalysts (see Figure S2); which indicates that this cannot be the only reason for the reduction of the intensity at 0.3 μs, found between the different spectra of these nanocomposites.

At 400 nm and 660 nm, P25-rGO 0% showed the highest initial transient absorption intensity, which dropped when the rGO concentration was increased even though the difference between

P25-rGO 0.5% and 1% was insignificant. Comparing the transient absorption kinetics at 400 nm, a slower decay and longer lifetime were observed for P25-rGO 0%. At 660 nm, P25-rGO 0.5% and 1%, showed a steady transient absorption.

On comparing the transient absorption spectra of the rGO based TiO_2 photocalysts under N_2 atmosphere in the presence of CH_3OH as a hole scavenger (see Figure 3), two different trends were observed. The transient absorption spectra of pure TiO_2 and P25-rGO 0.1% showed a poor intensity-response along the whole analyzed spectra, being the registered signal at 0.3 μs after the excitation very low. Subsequently the intensity rose until about 5 μs and remained steady thereafter. However, when P25-rGO 0.5% and P25-rGO 1% are considered, a complete different trend was noted. For these two nanocomposites, the transient absorption intensity showed its maximum values at 0.3 μs after the laser excitation. Subsequently, a continuous decrease of the intensity was observed up to 30 μs. Besides, when the absorption intensity in the 440-700 nm range was compared, it was noteworthy that final intensities of pure TiO_2 and P25-rGO 0.1% were very similar to the initial transient absorption intensities shown by P25-rGO 0.5% and P25-rGO 1% nanocomposites. This result might correspond to the maximum amount of photogenerated charge carriers (mainly electrons) which were able to be trapped in the TiO_2 framework. The fact that the maximum intensity was reached faster in the case of P25-rGO 0.5% and 1% could be attributed to the role played by rGO as an electron acceptor. In this sense, electrons would be transferred from TiO_2 to rGO, promoting the creation of sites where electrons can be injected by α-hydroxyalkyl radicals, and therefore achieving an enhancement of the photonic efficiency [6]. The drop of the transient intensity over time shown by P25-rGO 0.5% and 1% was probably caused by an excessive amount of rGO acting as a recombination center as previously reported [39, 65]. Furthermore, knowing that the particles have a size of 22 nm and assuming a molecular weight of 12.01 $g \cdot mol^{-1}$ for rGO (the actual value should be higher because of the presence of remaining oxygenated functional groups) a concentration ratio atom.% of 0.009 was calculated for the photocatalyst P25 with an rGO relative mass concentration of 0.1%, which is really close to the optimal ratio according to the linear dependency reported by Bloh et al. [65]. However, the transient absorption intensity just after excitation at 400 nm, related to the amount of photogenerated holes, was higher in the case of P25-rGO 0.5% (see Figure 3).

In comparison to the spectra of the nanocomposites obtained under N_2 atmosphere, those obtained under N_2-CH_3OH atmosphere changed radically. Immediately after the laser excitation a sharp increase of the transient intensity at 660 nm was detected, reaching a plateau at ~ 10 μs for both P25-rGO 0% and 0.1%. The higher intensity of the 660 nm signal reached by P25-rGO 0.1%, associated to a higher concentration of electrons, supports the discussion made above that about 0.1% is the optimal rGO mass concentration. Regarding P25-rGO 0.5% and 1% nanocomposites, the absorption signals at 660 nm were slightly higher, the lifetime of charge carriers was increased and the decay kinetics seemed to be slower than in the absence of

CH_3OH. In contrast to the transient absorption spectra collected in the absence of any scavenger, it could be noticed that the transient absorption intensity was higher when rGO was incorporated despite the shielding effect due to higher ground state absorption. This fact could be ascribed to a higher charge carrier concentration owing to a better charge separation thanks to the role of reduced graphene oxide as an electron acceptor. Therefore, the reduction of the transient absorption intensity observed upon increasing the rGO amount, under N_2 atmosphere, could not be attributed to the reduction of the path length or to the light-block effect.

For an in-depth understanding of the photogenerated charge carriers in the different rGO based TiO_2 nanocomposites, the transient absorption spectra was recorded under O_2 atmosphere and these spectra are shown in Figure 4. Oxygen is a well-known electron acceptor and therefore, an increase of the photogenerated holes signal should be detected.

On comparing the transient absorption spectra for pure TiO_2 obtained under N_2 and O_2 atmosphere (Figures 2 and 4), no changes in the transient spectra shape could be observed and the transient absorption intensity over the whole wavelength range was slightly reduced. This means that the signal could be related to strongly trapped electrons or electrons trapped far from the surface. However, in the case of the modified TiO_2 with rGO the spectra showed a different shape in the presence of the electron scavenger. Under O_2 atmosphere the intensity is slightly higher and it increases with the wavelength. These slight red-shift of the spectra compared to those under N_2 was related to electrons trapped away from the surface [55].

Regarding P25-rGO 0% at 660 nm, the transient absorption signal of pure TiO_2 experienced a fast decay, becoming the intensity lower than that of P25-rGO 0.1% at 5 μs after the laser excitation, reaching values close to the ones obtained in the case of P25-rGO 0.5% and 1% before 90 μs.

Based on these results, two different processes, depicted in Figure S3, could be described in the presence of hole and electron scavengers under UV irradiation. In the presence of N_2 and a hole scavenger, Figure S3 A, holes are trapped by methanol while electron are transferred to rGO. On the other hand, in the presence of O_2 as electron scavenger [66], Figure S3 B, a competitive transfer of the electrons to O_2 and rGO takes place. In the last process, holes react with adsorbed water to produce hydroxyl radicals that will further oxidize organic compounds.

To study the influence of the rGO content on the free electrons, the transient absorption signal was measured at 980 nm after exciting at 355 nm with an energy of ~2.2 $mJ \cdot cm^{-2}$. An infrared laser diode with an output power of 1 W was used as analyzing light to achieve a high light level. According to the study carried out by Yoshihara et al. [57], the signal detected at this wavelength is primarily ascribed to free electrons in the bulk of the photocatalyst. The transient absorption at 980 nm was measured under different atmospheres (data not shown here) but only a signal was detected when methanol was used as hole scavenger in N_2 atmosphere, Figure 5.

The highest transient absorption was observed for P25-rGO 0% which indicated a greater amount of free electrons. Regarding the TiO_2 coupled to rGO, the smallest signal was detected for P25-rGO 0.5% whereas the absorption values for P25-rGO with 0.1 and 1% were half the value reached by P25-rGO 0%. This further evinces the transfer of electrons from the valence band of TiO_2 to the rGO surface, reducing the amount of free and trapped electrons.

Then, to verify that electrons are not photogenerated in rGO and further transfer to the conduction band of TiO_2, the different composites were excited by a 450 nm pulse with an energy of ~2.1 $mJ \cdot cm^{-2}$ and using a 475 nm filter to prevent the catalysts from absorbing the probe light. Figure S4 shows the time profiles of the transient absorption at 560 and 660 nm for the studied TiO_2-rGO nanocomposites and under different experimental conditions. Since no signal was detected in none of the different atmospheres, not even in the presence of methanol, photogeneration of charge carriers in P25-rGO upon 450 nm excitation could be neglected.

3.2.1 Effect of rGO:TiO_2 doping ratio on charge carrier kinetics in the absence of hole and electron scavenger

In previous studies, the transient absorption decay kinetics related to trapped charge carriers were analyzed fitting the decay curves to second order kinetics to represent the recombination of electron-hole pairs [37, 55, 60, 67, 68]. However, as discussed by Sieland and coworkers [46] second order kinetics cannot be used to describe bimolecular recombination over the entire time domain; it will only fit well if the chosen time window is appropriate and fitting parameters depicting the residual signal are included. That is the reason why they used an empirical equation based on fractal surfaces to study charge carriers dynamics. In this model, equation 2, the second order rate constant *k* was replaced by a rate coefficient, k_f, and a time dependent factor, t^{-h}, where *h* represents the fractal dimension of the surface and A represents the height of the transient signal:

$$\Delta J = \frac{A(1-h)}{(1-h) + Ak_f t^{1-h}} \qquad (2)$$

The advantage of using this model is the possibility to describe charge carrier dynamics over all the observed time domains and excitation energies. In this study, carried out in the microsecond time scale, the recombination of trapped photogenerated holes and electrons was considered according to equation 3:

$$e^-_{tr} + h^+_{tr} \xrightarrow{k_f} heat \qquad (3)$$

The deviation assumes that the rate of the underlying process is given by $r = k_f t^{-h} N^2$, where N is the number of charge carriers.

The time profiles of the transient absorption in the absence and presence of scavengers were fitted using equation 2. In order to compare the kinetic parameters obtained from the fittings, an *h* value of 0.57 was taken. This *h* parameter was calculated as the average of the *h* values obtained from the fits without keeping constant this parameter. The calculated *h* value is closed to 0.5, the theoretical value for A+B reactions on square lattices at long times [46]. However, the h value is slightly higher because the fractal surface of the powder is more complex than a square even surface since the small particles tend to agglomerate.

Under N_2 atmosphere it was observed that the initial transient absorption in the region between 450 and 700 nm dropped upon increasing the rGO concentration. To prove that this decrease was caused by the electron transfer process to rGO, in Table 3 the k_f values obtained from the fittings for every P25-rGO nanocomposite were shown together with the initial absorbance ($\log I/I_0$) (under N_2 atmosphere). At 390 and 400 nm both the initial absorbance and the rate coefficient remain practically unchanged. However, for those wavelengths at which the absorbance of trapped electrons was more important, the initial absorbance decreased exponentially as the k_f value increased. These results confirmed that electrons are transferred from TiO_2 to rGO, probably in the picosecond time scale [6, 58, 61].

Comparing rate constants (k_f) in N_2 atmosphere, Table 3, it could be seen that when P25-rGO 0% is considered, k_f coefficients are very similar regardless of the wavelength. However, regarding the P25-rGO nanocomposites, as the wavelength increases, the k_f values increases with the rGO content, becoming between four and nine times higher than those for P25-rGO 0% at 660 nm. However the k_f values obtained at 390 and 400 nm, previously ascribed mainly to trapped holes, were close to the value obtained for the bare TiO_2. For none of the TiO_2-rGO nanocomposites the k_f coefficient was reduced compared to the bare TiO_2, indicating that rGO could not prevent the hole recombination despite the fact it favored the transfer of electrons. Slightly higher values of k_f were observed at 390 and 400 nm for P25-rGO 1%. Patrocinio et al. [58] reported a faster decay process of the transient absorption signal at 400 nm when Pt, an electron acceptor like rGO, was added to TiO_2, ascribed to the migration of holes between different trapping sites after being the electrons transferred to Pt. On the other hand, this effect could also be related to the role played by the rGO as recombination centers in the absence of any scavenger [28].

3.2.2 Charge carrier kinetics in the presence of hole and electron scavenger

In the presence of CH_3OH and O_2 as hole and electron scavenger, respectively, the differences among the kinetic parameters obtained for the nanocomposites are negligible (see Figure 6 A).

The fact that similar k_f values were obtained at 400 nm in the presence and absence of CH_3OH further supports that the absorption at this wavelength corresponds to unreactive deeply trapped holes [6, 58]. Values of k_f for P25-rGO 0% and 0.1% could not be calculated under a N_2 atmosphere saturated in CH_3OH since the transient absorption signals reached a plateau immediately after the laser pulse. On the other hand, in the presence of an electron scavenger, P25-rGO 0% showed the highest rate coefficient at 660 nm, which indicates that the recombination rate of electron-hole pairs was higher than in the case of P25-rGO nanocomposites because of the transfer of electrons to rGO and further to oxygen. However, in the case of P25-rGO 0.1% the lowest decay constant was obtained when the electron scavenger was used. So, as was argued before, a mass concentration of 0.1% of rGO could be the optimal ratio and higher content would lead to higher recombination rates.

In comparison to *A* values estimated in N_2, *A* values obtained in O_2 for P25-rGO 0% and P25-rGO 0.1% decreased. This means that electron transfer to rGO in not as favored under O_2 atmosphere as under N_2 atmosphere, leading to lower differences in the photocatalytic activity reached by the different photocatalysts when there is an excess of dissolved O_2 in the reaction volume.

Regarding *A* values calculated at 390 and 400 nm, P25-rGO 0.5% exhibited a maximum in spite of being the estimated k_f values equal to those obtained for other nanocomposites. Furthermore, P25-rGO 0.5% yielded the highest *A* values at 400nm, regardless of the atmosphere or scavenger used, (see Figure 6 B) related to a higher concentration of photogenerated holes. That is the result of a greater transfer of electrons from TiO_2 to rGO as evinced by the lowest calculated A values at 660 nm.

3.3 Photocatalytic activity

To verify the advantages of modifying TiO_2 with rGO, the photocatalytic degradation of dicholoroacetic acid (DCA) in aqueous suspension was studied. TOC and DCA conversions achieved by each photocatalyst after 150 minutes and the initial reaction rate are shown in Table 4. Also, time evolution of DCA and Cl^- concentrations for the different nanocomposites are depicted in Figure S5. The highest TOC and DCA conversions were obtained for P25-rGO 0.1%, 93.3% and 94.6%, respectively. In order to explain these results, the rate coefficient k_f estimated at 660 nm under an O_2 atmosphere and DCA degradation rate were plotted against the rGO (%) mass concentration in Figure 7. The fastest photodegradation rate was obtained for P25-rGO 0.1%, being 1.22 times higher than the initial photodegradation rate of P25-rGO 0%. What is more, the fastest initial reaction rate coincided with the lowest k_f value, which indicates that the faster DCA removal was due to a more efficient separation of electron-hole pairs preventing their recombination. In addition, it could also be related to the longer lifetimes of the charge carriers. However, lower TOC and DCA conversions were detected for P25-rGO 0.5% and P25-rGO 1%,

around 80% and 75% of TOC conversion respectively. Two reasons might be mentioned to explain these values. Firstly, an excessive amount of rGO, might act as recombination centers. And secondly, light-block effects may occur on account of an excess of rGO that can block incident light that arrives at the nanoparticles suspended in the reaction medium. In conclusion, the results obtained using transient absorption spectroscopy in the microsecond time scale were related to the photocatalytic activity. All in all, P25-rGO 0.1% seemed to be the optimal rGO mass concentration under the studied conditions, leading to the highest photocatalytic DCA and TOC molar conversion values.

4. CONCLUSIONS

Even though a lot of studies concerning the activity of TiO_2-rGO nanocomposites have been reported, a clear understanding of the role played by rGO is essential to improve the design of these nanocomposites. In this study, a decrease of the transient absorption signal in the 450-700 nm region, under a nitrogen atmosphere, is observed in the microsecond scale when the rGO mass doping ratio was gradually increased. The data were fitted to a model based on fractal surfaces. The smaller values of the initial absorbance were related to the very high rate constants (k_f) obtained in the region between 450 and 700, concluding that the electron transfer from the conduction band of TiO_2 to rGO took place during the dead time of the measurement. Furthermore, the rate constant values calculated at 400 nm were very similar for the different nanocomposites indicating that an increase of the lifetime of photogenerated holes could not be confirmed. This might be because these rate constants correspond to unreactive deeply trapped holes

In the presence of a hole scavenger such as methanol, recombination of the charged carriers could be reduced. P25-rGO 0.1% showed the greatest transient absorption at 660 nm after 10 μs whereas P25-rGO 0.5% and 1% yielded the highest absorption signals just after the laser pulse, which dropped subsequently. This decay could be related to an excess of rGO that can act as recombination centers.

To analyze the effect of the rGO concentration on the free electrons, the transient absorption signal at 980 nm was measured. Only when methanol was used as a hole scavenger a signal was detected. Smaller transient signals were detected when rGO was coupled to TiO_2 which evinced the transfer of electrons from the conduction band of TiO_2 to the surface of rGO. No sensitization effect of rGO was observed in this study when the samples were excited at 450 nm. The photocatalytic degradation of dichloroacetic acid was also evaluated for the analyzed nanocomposites and the nanocomposite P25-rGO 0.1% yielded the best molar conversions and the best initial photodegradation rate.

Acknowledgements

This work has been supported by the Spanish Plan Nacional de I+D+i through the project CTM2015-64895-R. Alvaro Tolosana-Moranchel thanks to Ministerio de Educación, Cultura y Deporte for his FPU grant (FPU14/01605) and (EST16/00065). The authors are also grateful to Technical Research Support Unit of Instituto de Catálisis y Petroleoquímica (CSIC).

5. REFERENCES

[1] L.L. Tan, S.P. Chai, A.R. Mohamed, Synthesis and applications of graphene-based TiO 2 photocatalysts, ChemSusChem, 5 (2012) 1868-1882.
[2] L.L. Tan, W.J. Ong, S.P. Chai, A.R. Mohamed, Visible-light-activated oxygen-rich TiO<inf>2</inf> as next generation photocatalyst: Importance of annealing temperature on the photoactivity toward reduction of carbon dioxide, Chemical Engineering Journal, 283 (2016) 1254-1263.
[3] S. Malato, P. Fernández-Ibáñez, M.I. Maldonado, J. Blanco, W. Gernjak, Decontamination and disinfection of water by solar photocatalysis: Recent overview and trends, Catalysis Today, 147 (2009) 1-59.
[4] N.H. Tran, M. Reinhard, K.Y.H. Gin, Occurrence and fate of emerging contaminants in municipal wastewater treatment plants from different geographical regions-a review, Water Research, 133 (2018) 182-207.
[5] J. Carbajo, Thesis Dissertation: Application of Solar Assisted Photodegradationof Organic Pollutants in Aqueous Phase with Nanostructured Titania Catalysts, in, Universidad Autónoma de Madrid, Spain, 2013.
[6] J. Schneider, M. Matsuoka, M. Takeuchi, J. Zhang, Y. Horiuchi, M. Anpo, D.W. Bahnemann, Understanding TiO2 Photocatalysis: Mechanisms and Materials, Chemical Reviews, 114 (2014) 9919-9986.
[7] J.Z. Bloh, R. Dillert, D.W. Bahnemann, Ruthenium-modified zinc oxide, a highly active vis-photocatalyst: the nature and reactivity of photoactive centres, Physical Chemistry Chemical Physics, 16 (2014) 5833-5845.
[8] A. Engel, J. Große, R. Dillert, D.W. Bahnemann, The Influence of Irradiance and Humidity on the Photocatalytic Conversion of Nitrogen(II) Oxide, Journal of Advanced Oxidation Technologies, 18 (2015) 195-203.
[9] M. Martín-Sómer, C. Pablos, R. van Grieken, J. Marugán, Influence of light distribution on the performance of photocatalytic reactors: LED vs mercury lamps, Applied Catalysis B: Environmental, 215 (2017) 1-7.
[10] M. Martín-Sómer, B. Vega, C. Pablos, R. van Grieken, J. Marugán, Wavelength dependence of the efficiency of photocatalytic processes for water treatment, Applied Catalysis B: Environmental, 221 (2018) 258-265.
[11] P. Fernández-Ibáñez, M.I. Polo-López, S. Malato, S. Wadhwa, J.W.J. Hamilton, P.S.M. Dunlop, R. D'Sa, E. Magee, K. O'Shea, D.D. Dionysiou, J.A. Byrne, Solar photocatalytic disinfection of water using titanium dioxide graphene composites, Chemical Engineering Journal, 261 (2015) 36-44.
[12] K. Ullah, A. Ali, S. Ye, L. Zhu, W.C. Oh, Microwave-assisted synthesis of Pt-graphene/TiO2 nanocomposites and their efficiency in assisting hydrogen evolution from water in the presence of sacrificial agents, Science of Advanced Materials, 7 (2015) 606-614.
[13] B. Gupta, A.A. Melvin, TiO2/RGO composites: Its achievement and factors involved in hydrogen production, Renewable and Sustainable Energy Reviews, 76 (2017) 1384-1392.
[14] X. Chen, S. Shen, L. Guo, S.S. Mao, Semiconductor-based Photocatalytic Hydrogen Generation, Chemical Reviews, 110 (2010) 6503-6570.
[15] A. Kudo, Y. Miseki, Heterogeneous photocatalyst materials for water splitting, Chemical Society Reviews, 38 (2009) 253-278.
[16] A.V. Puga, Photocatalytic production of hydrogen from biomass-derived feedstocks, Coordination Chemistry Reviews, 315 (2016) 1-66.

[17] P. Ribao, M.J. Rivero, I. Ortiz, TiO2 structures doped with noble metals and/or graphene oxide to improve the photocatalytic degradation of dichloroacetic acid, Environmental Science and Pollution Research, 24 (2017) 12628-12637.
[18] M. Sharma, S. Vaidya, A.K. Ganguli, Enhanced photocatalytic activity of g-C3N4-TiO2 nanocomposites for degradation of Rhodamine B dye, Journal of Photochemistry and Photobiology A: Chemistry, 335 (2017) 287-293.
[19] T. Liu, B. Liu, L. Yang, X. Ma, H. Li, S. Yin, T. Sato, T. Sekino, Y. Wang, RGO/Ag2S/TiO2 ternary heterojunctions with highly enhanced UV-NIR photocatalytic activity and stability, Applied Catalysis B: Environmental, 204 (2017) 593-601.
[20] Q. Wang, N. Zhu, E. Liu, C. Zhang, J.C. Crittenden, Y. Zhang, Y. Cong, Fabrication of visible-light active Fe2O3-GQDs/NF-TiO2 composite film with highly enhanced photoelectrocatalytic performance, Applied Catalysis B: Environmental, 205 (2017) 347-356.
[21] J.A. Anderson, Photocatalytic nitrate reduction over Au/TiO2, Catalysis Today, 175 (2011) 316-321.
[22] H. Zhang, X. Lv, Y. Li, Y. Wang, J. Li, P25-Graphene Composite as a High Performance Photocatalyst, ACS Nano, 4 (2009) 380-386.
[23] J. Wang, S.A. Kondrat, Y. Wang, G.L. Brett, C. Giles, J.K. Bartley, L. Lu, Q. Liu, C.J. Kiely, G.J. Hutchings, Au–Pd Nanoparticles Dispersed on Composite Titania/Graphene Oxide-Supports as a Highly Active Oxidation Catalyst, ACS Catalysis, 5 (2015) 3575-3587.
[24] G. Kim, Y. Park, G.-h. Moon, W. Choi, CHAPTER 5 Photoexcitation in Pure and Modified Semiconductor Photocatalysts, in: Photocatalysis: Fundamentals and Perspectives, The Royal Society of Chemistry, 2016, pp. 110-128.
[25] S. Ouyang, H. Xu, CHAPTER 11 New Materials for Degradation of Organics, in: Photocatalysis: Fundamentals and Perspectives, The Royal Society of Chemistry, 2016, pp. 252-294.
[26] X. Li, R. Shen, S. Ma, X. Chen, J. Xie, Graphene-based heterojunction photocatalysts, Applied Surface Science, 430 (2018) 53-107.
[27] M. Faraldos, A. Bahamonde, Environmental applications of titania-graphene photocatalysts, Catalysis Today, 285 (2017) 13-28.
[28] M. Minella, F. Sordello, C. Minero, Photocatalytic process in TiO2/graphene hybrid materials. Evidence of charge separation by electron transfer from reduced graphene oxide to TiO2, Catalysis Today, 281 (2017) 29-37.
[29] H. Adamu, P. Dubey, J.A. Anderson, Probing the role of thermally reduced graphene oxide in enhancing performance of TiO2 in photocatalytic phenol removal from aqueous environments, Chemical Engineering Journal, 284 (2016) 380-388.
[30] Q. Xiang, J. Yu, M. Jaroniec, Enhanced photocatalytic H2-production activity of graphene-modified titania nanosheets, Nanoscale, 3 (2011) 3670-3678.
[31] M. Shafaee, E.K. Goharshadi, M. Mashreghi, M. Sadeghinia, TiO2 nanoparticles and TiO2@graphene quantum dots nancomposites as effective visible/solar light photocatalysts, Journal of Photochemistry and Photobiology A: Chemistry, 357 (2018) 90-102.
[32] R. Shahbazi, A. Payan, M. Fattahi, Preparation, evaluations and operating conditions optimization of nano TiO2 over graphene based materials as the photocatalyst for degradation of phenol, Journal of Photochemistry and Photobiology A: Chemistry, 364 (2018) 564-576.
[33] Y. Xu, Y. Li, P. Wang, X. Wang, H. Yu, Highly efficient dual cocatalyst-modified TiO2 photocatalyst: RGO as electron-transfer mediator and MoSx as H2-evolution active site, Applied Surface Science, 430 (2018) 176-183.
[34] Z. Zhu, F. Zhou, S. Zhan, Y. Tian, Q. He, Study on the bactericidal performance of graphene/TiO2 composite photocatalyst in the coating of PEVE, Applied Surface Science, 430 (2018) 116-124.
[35] M. Minella, M. Demontis, M. Sarro, F. Sordello, P. Calza, C. Minero, Photochemical stability and reactivity of graphene oxide, Journal of Materials Science, 50 (2015) 2399-2409.
[36] T.-F. Yeh, H. Teng, Graphite Oxide with Different Oxygen Contents as Photocatalysts for Hydrogen and Oxygen Evolution from Water, ECS Transactions, 41 (2012) 7-26.

[37] J. Schneider, K. Nikitin, M. Wark, D.W. Bahnemann, R. Marschall, Improved charge carrier separation in barium tantalate composites investigated by laser flash photolysis, Physical Chemistry Chemical Physics, 18 (2016) 10719-10726.
[38] Y. Tamaki, A. Furube, M. Murai, K. Hara, R. Katoh, M. Tachiya, Dynamics of efficient electron-hole separation in TiO2 nanoparticles revealed by femtosecond transient absorption spectroscopy under the weak-excitation condition, Physical Chemistry Chemical Physics, 9 (2007) 1453-1460.
[39] A. Morais, C. Longo, J.R. Araujo, M. Barroso, J.R. Durrant, A.F. Nogueira, Nanocrystalline anatase TiO2/reduced graphene oxide composite films as photoanodes for photoelectrochemical water splitting studies: the role of reduced graphene oxide, Physical Chemistry Chemical Physics, 18 (2016) 2608-2616.
[40] P. Wang, N.M. Dimitrijevic, A.Y. Chang, R.D. Schaller, Y. Liu, T. Rajh, E.A. Rozhkova, Photoinduced Electron Transfer Pathways in Hydrogen-Evolving Reduced Graphene Oxide-Boosted Hybrid Nano-Bio Catalyst, ACS Nano, 8 (2014) 7995-8002.
[41] J. Marugán, D. Hufschmidt, G. Sagawe, V. Selzer, D. Bahnemann, Optical density and photonic efficiency of silica-supported TiO2 photocatalysts, Water Research, 40 (2006) 833-839.
[42] H.N.D. Zhebo Chen, Eric Miller, Photoelectrochemical Water Splitting Standards, Experimental Methods, and Protocols, Springer New York, 2013.
[43] R.L.Z. R. Jenkins, Introduction to X-Ray powder Diffractometry, John Wisley & Sons Inc., New York, 1996.
[44] R.A. Spurr, H. Myers, Quantitative Analysis of Anatase-Rutile Mixtures with an X-Ray Diffractometer, Analytical Chemistry, 29 (1957) 760-762.
[45] S. Brunauer, P.H. Emmett, E. Teller, Adsorption of Gases in Multimolecular Layers, Journal of the American Chemical Society, 60 (1938) 309-319.
[46] F. Sieland, J. Schneider, D.W. Bahnemann, Fractal Charge Carrier Kinetics in TiO2, The Journal of Physical Chemistry C, 121 (2017) 24282-24291.
[47] A. Tolosana-Moranchel, J.A. Casas, J. Carbajo, M. Faraldos, A. Bahamonde, Influence of TiO2 optical parameters in a slurry photocatalytic reactor: Kinetic modelling, Applied Catalysis B: Environmental, 200 (2017) 164-173.
[48] X. Rong, F. Qiu, C. Zhang, L. Fu, Y. Wang, D. Yang, Preparation, characterization and photocatalytic application of TiO2–graphene photocatalyst under visible light irradiation, Ceramics International, 41 (2015) 2502-2511.
[49] N.J. Bell, Y.H. Ng, A. Du, H. Coster, S.C. Smith, R. Amal, Understanding the Enhancement in Photoelectrochemical Properties of Photocatalytically Prepared TiO2-Reduced Graphene Oxide Composite, The Journal of Physical Chemistry C, 115 (2011) 6004-6009.
[50] A.W. Morawski, E. Kusiak-Nejman, A. Wanag, J. Kapica-Kozar, R.J. Wróbel, B. Ohtani, M. Aksienionek, L. Lipińska, Photocatalytic degradation of acetic acid in the presence of visible light-active TiO2-reduced graphene oxide photocatalysts, Catalysis Today, 280 (2017) 108-113.
[51] S. Kaniyankandy, S.N. Achary, S. Rawalekar, H.N. Ghosh, Ultrafast Relaxation Dynamics in Graphene Oxide: Evidence of Electron Trapping, The Journal of Physical Chemistry C, 115 (2011) 19110-19116.
[52] B.R. Cruz-Ortiz, J.W.J. Hamilton, C. Pablos, L. Díaz-Jiménez, D.A. Cortés-Hernández, P.K. Sharma, M. Castro-Alférez, P. Fernández-Ibañez, P.S.M. Dunlop, J.A. Byrne, Mechanism of photocatalytic disinfection using titania-graphene composites under UV and visible irradiation, Chemical Engineering Journal, 316 (2017) 179-186.
[53] P. Calza, C. Hadjicostas, V.A. Sakkas, M. Sarro, C. Minero, C. Medana, T.A. Albanis, Photocatalytic transformation of the antipsychotic drug risperidone in aqueous media on reduced graphene oxide—TiO2 composites, Applied Catalysis B: Environmental, 183 (2016) 96-106.
[54] D.W. Bahnemann, M. Hilgendorff, R. Memming, Charge Carrier Dynamics at TiO2 Particles: Reactivity of Free and Trapped Holes, The Journal of Physical Chemistry B, 101 (1997) 4265-4275.
[55] A. Furube, T. Asahi, H. Masuhara, H. Yamashita, M. Anpo, Charge Carrier Dynamics of Standard TiO2 Catalysts Revealed by Femtosecond Diffuse Reflectance Spectroscopy, The Journal of Physical Chemistry B, 103 (1999) 3120-3127.

[56] Y. Tamaki, A. Furube, R. Katoh, M. Murai, K. Hara, H. Arakawa, M. Tachiya, Trapping dynamics of electrons and holes in a nanocrystalline TiO2 film revealed by femtosecond visible/near-infrared transient absorption spectroscopy, Comptes Rendus Chimie, 9 (2006) 268-274.
[57] T. Yoshihara, R. Katoh, A. Furube, Y. Tamaki, M. Murai, K. Hara, S. Murata, H. Arakawa, M. Tachiya, Identification of Reactive Species in Photoexcited Nanocrystalline TiO2 Films by Wide-Wavelength-Range (400−2500 nm) Transient Absorption Spectroscopy, The Journal of Physical Chemistry B, 108 (2004) 3817-3823.
[58] A.O.T. Patrocinio, J. Schneider, M.D. Franca, L.M. Santos, B.P. Caixeta, A.E.H. Machado, D.W. Bahnemann, Charge carrier dynamics and photocatalytic behavior of TiO2 nanopowders submitted to hydrothermal or conventional heat treatment, RSC Advances, 5 (2015) 70536-70545.
[59] F. Akihiro, A. Tsuyoshi, M. Hiroshi, Y. Hiromi, A. Masakazu, Femtosecond Diffuse Reflectance Spectroscopy on Some Standard TiO2 Powder Calalysts, Chemistry Letters, 26 (1997) 735-736.
[60] N. Serpone, D. Lawless, R. Khairutdinov, E. Pelizzetti, Subnanosecond Relaxation Dynamics in TiO2 Colloidal Sols (Particle Sizes Rp = 1.0-13.4 nm). Relevance to Heterogeneous Photocatalysis, The Journal of Physical Chemistry, 99 (1995) 16655-16661.
[61] F. Meng, J. Li, S.K. Cushing, J. Bright, M. Zhi, J.D. Rowley, Z. Hong, A. Manivannan, A.D. Bristow, N. Wu, Photocatalytic Water Oxidation by Hematite/Reduced Graphene Oxide Composites, ACS Catalysis, 3 (2013) 746-751.
[62] N. Liaros, S. Couris, E. Koudoumas, P.A. Loukakos, Ultrafast Processes in Graphene Oxide during Femtosecond Laser Excitation, The Journal of Physical Chemistry C, 120 (2016) 4104-4111.
[63] H.G. Baldoví, M. Álvaro, B. Ferrer, H. García, Photoinduced Charge Separation on the Microsecond Timescale in Graphene Oxide and Reduced Graphene Oxide Suspensions, ChemPhysChem, 17 (2016) 958-962.
[64] A. Furube, T. Asahi, H. Masuhara, H. Yamashita, M. Anpo, Direct observation of a picosecond charge separation process in photoexcited platinum-loaded TiO2 particles by femtosecond diffuse reflectance spectroscopy, Chemical Physics Letters, 336 (2001) 424-430.
[65] J.Z. Bloh, R. Dillert, D.W. Bahnemann, Designing optimal metal-doped photocatalysts: Correlation between photocatalytic activity, doping ratio, and particle size, Journal of Physical Chemistry C, 116 (2012) 25558-25562.
[66] H.H. Mohamed, R. Dillert, D.W. Bahnemann, Reaction dynamics of the transfer of stored electrons on TiO2 nanoparticles: A stopped flow study, Journal of Photochemistry and Photobiology A: Chemistry, 217 (2011) 271-274.
[67] B. Ohtani, Titania Photocatalysis beyond Recombination: A Critical Review, Catalysts, 3 (2013) 942.
[68] G. Rothenberger, J. Moser, M. Graetzel, N. Serpone, D.K. Sharma, Charge carrier trapping and recombination dynamics in small semiconductor particles, Journal of the American Chemical Society, 107 (1985) 8054-8059.

FIGURES

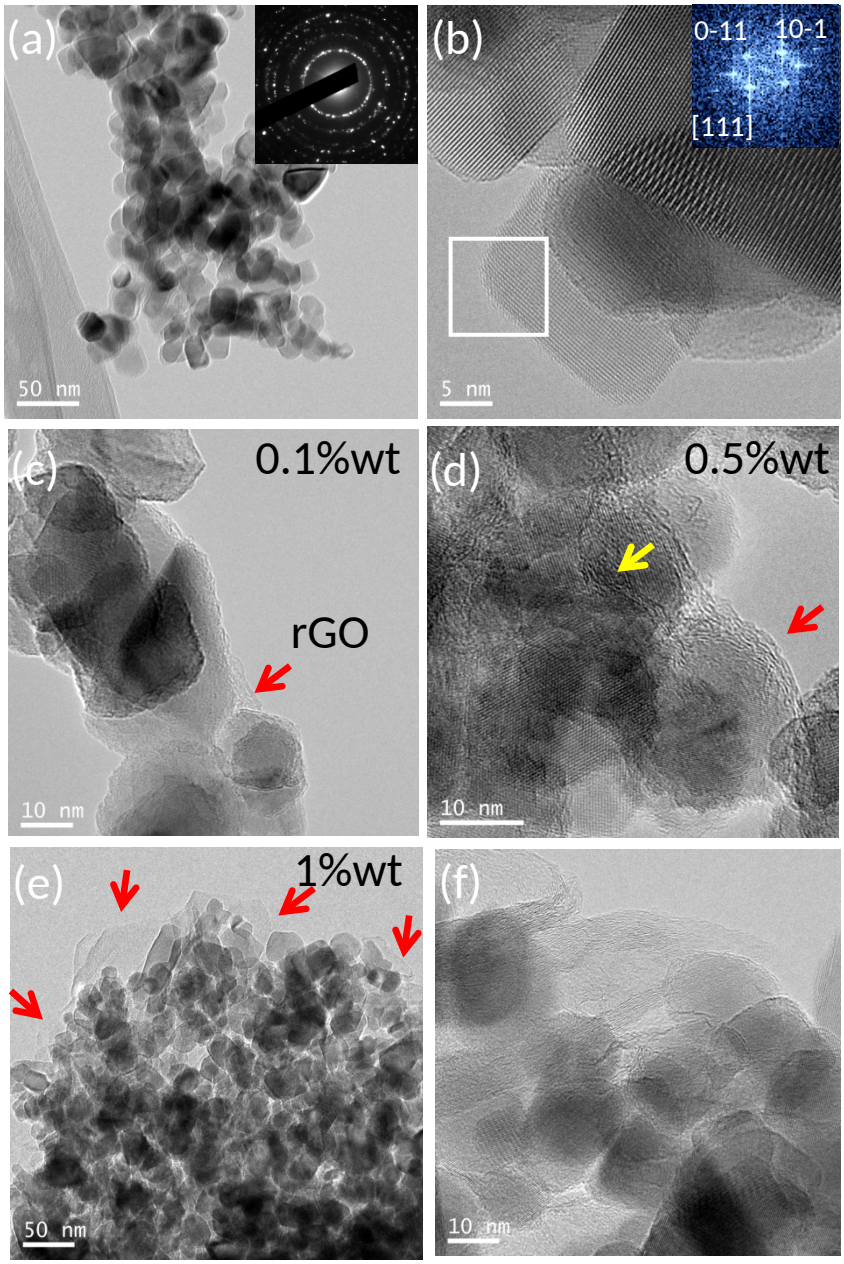

Figure 1. TEM images of the P25-rGO composites: (a) TEM image of P25-rGO 0% and the inset shows the SAED (Selected Area Electron Diffraction) pattern; (b) HRTEM micrograph of the TiO2 particles; (c) and (d) shows HRTEM micrographs of P25-rGO 0.1% and 0.5%, respectively; (e) and (f) are TEM and HRTEM images of P25-rGO 1%.

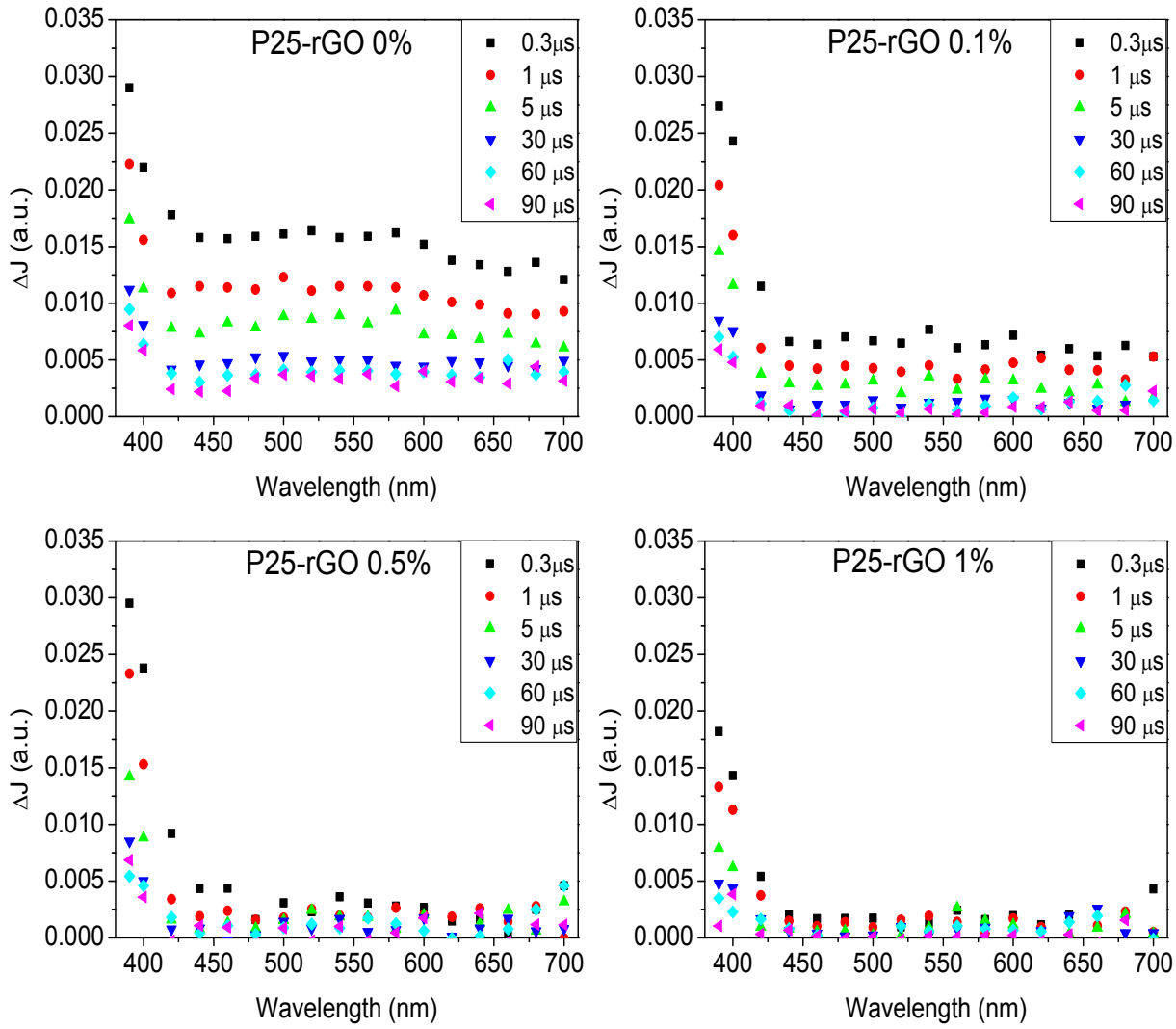

Figure 2. Transient Absorption spectra measured at various times after excitation (355 nm) for TiO_2 and TiO_2-rGO nanocomposites in N_2 atmosphere.

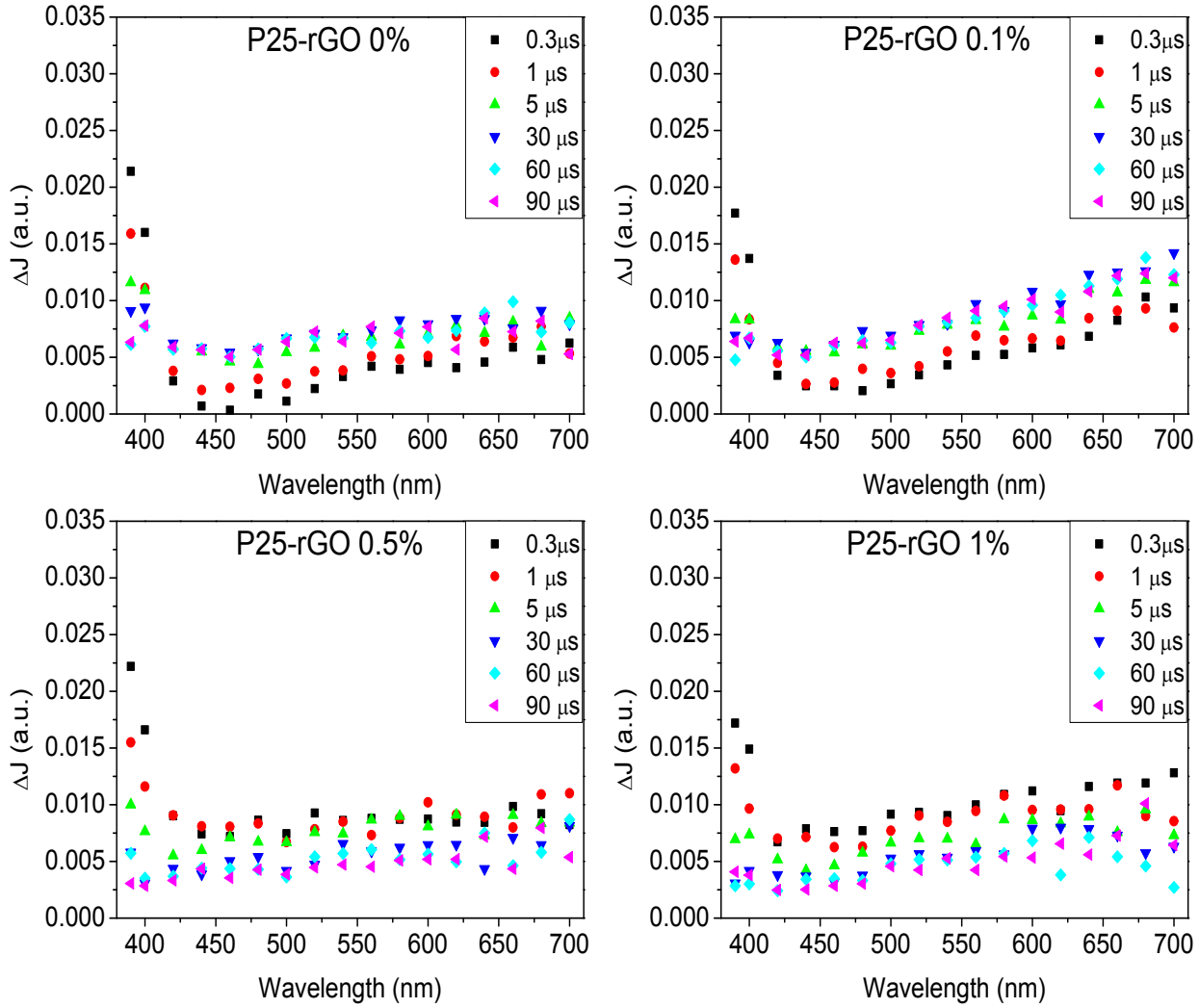

Figure 3. Transient absorption spectra measured at various times after excitation (355 nm) for TiO_2 and TiO_2-rGO nanocomposites in N_2-CH_3OH atmosphere.

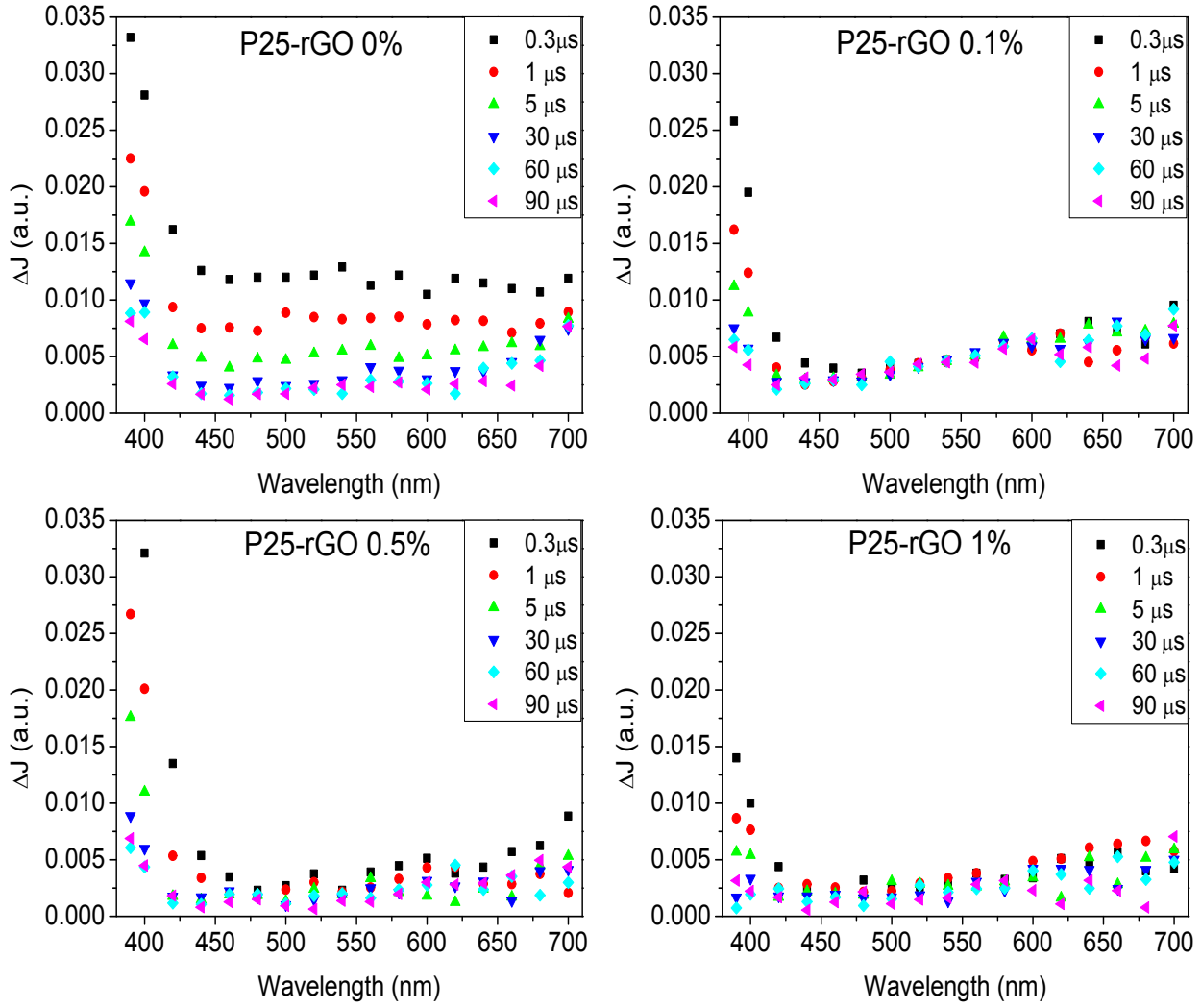

Figure 4. Transient absorption spectra measured at various times after excitation (355 nm) for TiO_2 and TiO_2-rGO nanocomposites in O_2 atmosphere.

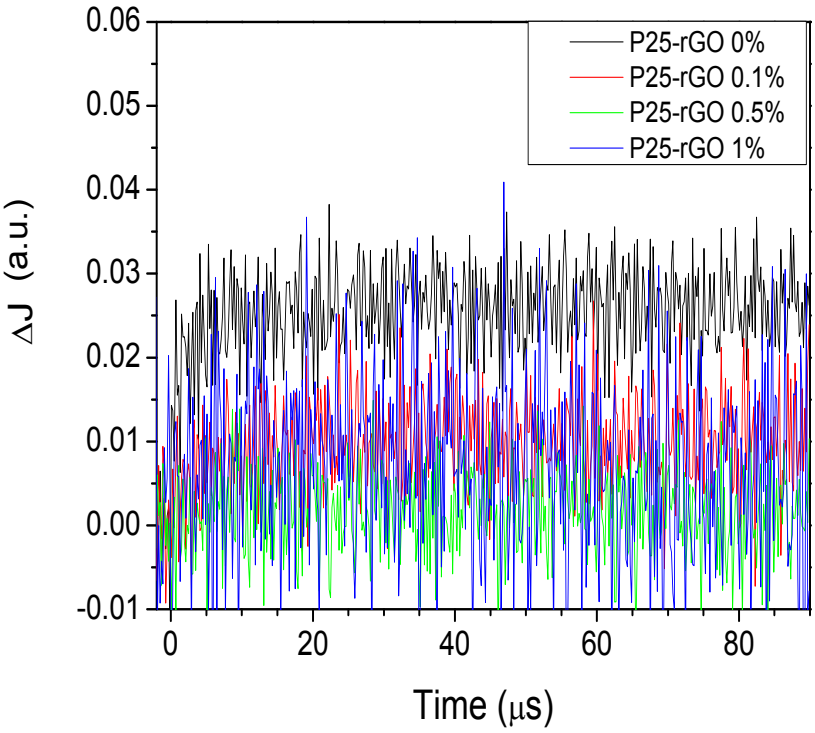

Figure 5. Time profiles of transient absorption at 980 nm for the studied nanocomposites under N_2 atmosphere in the presence of CH_3OH as hole scavenger.

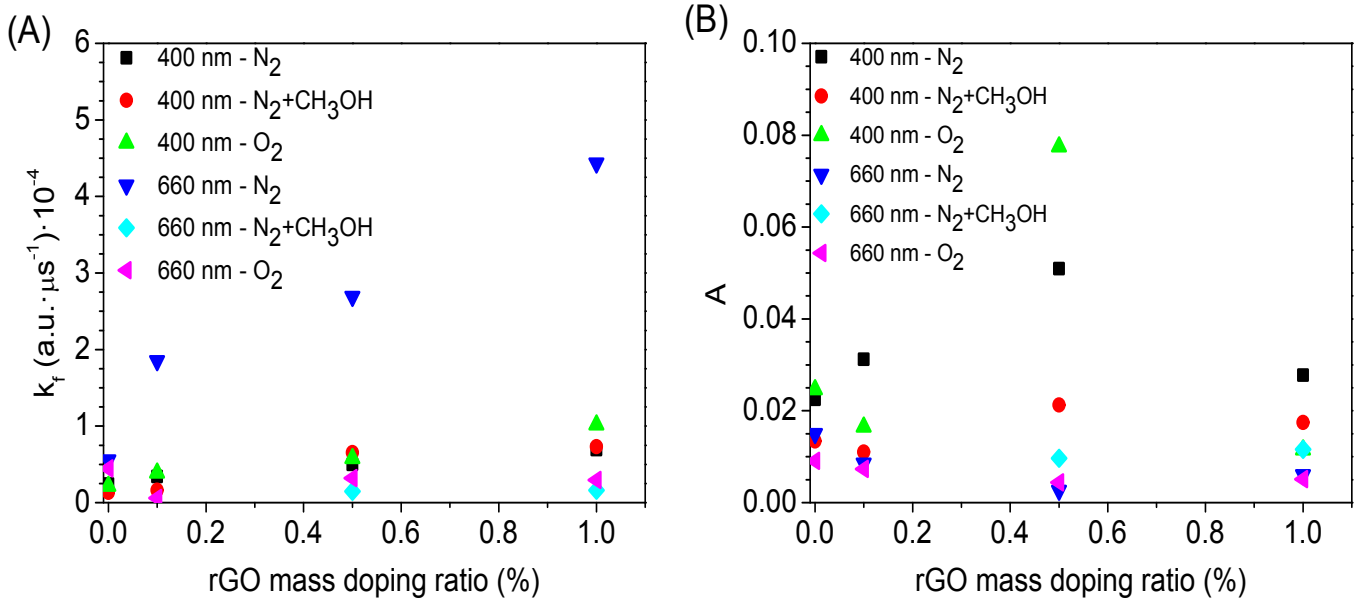

Figure 6. Estimated parameters for equation 2 of the transient decay signals dependent on the rGO (wt. %) mass concentration. kf at 400 and 660 nm under different atmospheres and using CH3OH as a hole scavenger (A) and A at 400 and 660 nm under different atmospheres and using CH3OH as a hole scavenger (B).

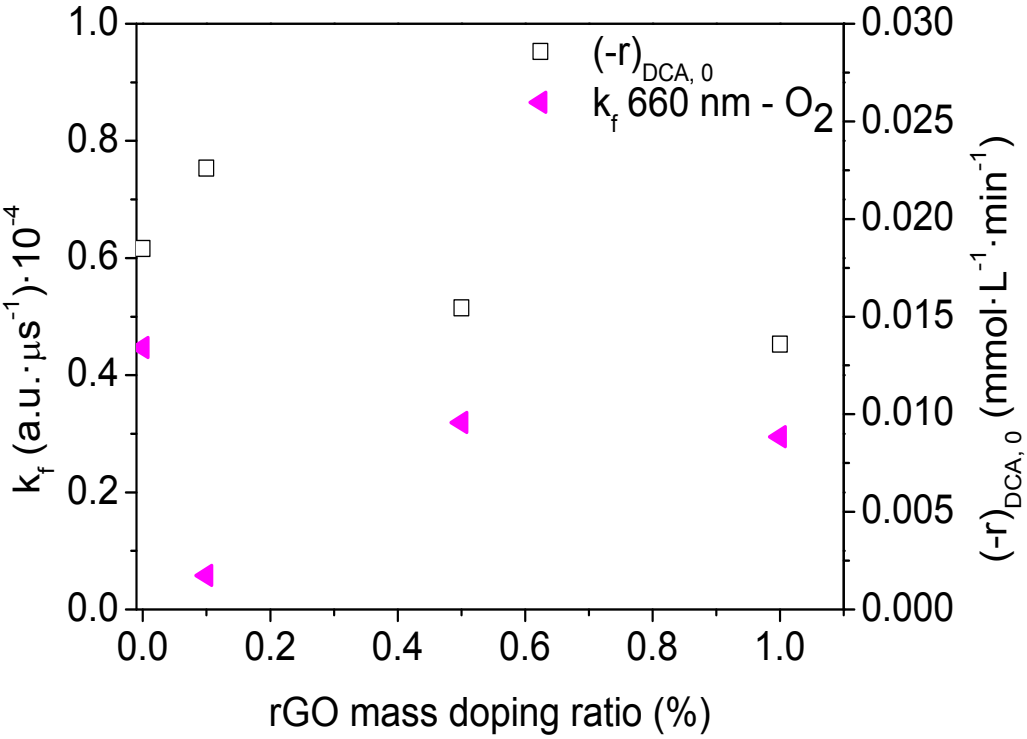

Figure 7. Rate coefficient k_f estimated at 660 nm under O_2 atmosphere and DCA degradation rate plotted against the rGO (wt. %) mass concentration.

TABLES

Table 1. Main physico-chemical properties of TiO_2 and TiO_2-rGO photocatalysts.

Photocatalyst	S_{BET}	Anatase	Rutile	$d_{Anatase}$	d_{Rutile}	Band gap	A_D/A_G*
	(m^2/g)	(%)	(%)	(nm)	(nm)	(eV)	a.u.
P25-rGO 0%	57	81	19	19.4	29.6	3.1	-
P25-rGO 0.1%	59	83	17	19.4	28.4	3.1	1.44
P25-rGO 0.5%	59	81	19	19.4	30.8	3.2	1.44
P25-rGO 1%	61	81	19	19.4	30.8	3.2	1.37

* The ratio A_D/A_G was 1.13 for GO

Table 2. Surface chemical composition of the nanocomposites studied by EDX.

	weight%			Std. Deviation		
	C	O	Ti	C	O	Ti
P25-rGO 0.5%	2.43	43.47	54.1	0.58	2.25	1.97
P25-rGO 1%	2.83	47.59	49.58	0.52	7.13	7.61

Table 3. Experimental initial absorbance at discrete wavelengths as a function of the calculated parameter k_f for the studied nanocomposites.

	Initial absorbance (u.a.)					
	390 nm	**400 nm**	**440 nm**	**540 nm**	**600 nm**	**660 nm**
P25-rGO 0%	0.013	0.010	0.007	0.007	0.007	0.006
P25-rGO 0.1%	0.012	0.011	0.003	0.003	0.003	0.002
P25-rGO 0.5%	0.013	0.010	0.002	0.002	0.001	0.000
P25-rGO 1%	0.008	0.006	0.001	0.001	0.001	0.000
	k_f (a.u.)					
	390 nm	**400 nm**	**440 nm**	**540 nm**	**600 nm**	**660 nm**
P25-rGO 0%	1914.8	2428.3	6580.5	5371.0	5371.0	5561.5
P25-rGO 0.1%	2845.8	3414.0	34583.1	21943.7	21943.7	18530.1
P25-rGO 0.5%	3338.7	4998.1	48208.6	45241.3	45241.3	26899.3
P25-rGO 1%	4526.9	6913.9	78326.8	30032.4	30032.4	44316.4

Table 4. DCA and TOC molar conversion reached after 150 minutes and initial degradation rates of DCA for the studied P25-rGO nanocomposites.

	X_{DCA} (%)	X_{TOC} (%)	$(-r)_{DCA,\,0}$ ($mmol \cdot L^{-1} \cdot min^{-1}$)	r^2
P25-rGO 0%	90.6	89.2	$1.85 \cdot 10^{-2}$	1.000
P25-rGO 0.1%	94.6	93.3	$2.26 \cdot 10^{-2}$	0.998
P25-rGO 0.5%	82.8	80.4	$1.55 \cdot 10^{-2}$	0.999
P25-rGO 1%	79.1	75.0	$1.36 \cdot 10^{-2}$	0.999

TiO_2-REDUCED GRAPHENE OXIDE NANOCOMPOSITES: MICROSECOND CHARGE CARRIER KINETICS

A. Tolosana-Moranchel[1], M. Faraldos[2], A. Bahamonde[2], L. Pascual[2], F. Sieland[3], J. Schneider[3], R. Dillert[3,4], D. W. Bahnemann[3,5]

[1]Departamento de Ingeniería Química, Facultad de Ciencias, C/ Francisco Tomás y Valiente 7, Universidad Autónoma de Madrid, 28049 Madrid (Spain).

[2]Instituto de Catálisis y Petroleoquímica, ICP-CSIC, C/ Marie Curie 2, 28049 Madrid (Spain).

[3]Institute of Technical Chemistry, Leibniz University Hannover, Callinstr. 5, 30167 Hannover,
Germany.

[4]Laboratorium für Nano- und Quantenengineering, Gottfried Wilhelm Leibniz Universität Hannover, Schneiderberg 39, 30167 Hannover, Germany.

[5]Laboratory of Photoactive Nanocomposite Materials, Department of Photonics, Faculty of Physics, Saint-Petersburg State University, Ulianovskaia str. 3, Peterhof, Saint-Petersburg 198504, Russia.

[1]Corresponding authors: e-mail address: alvaro.tolosana@uam.es, schneider@iftc.uni-hannover.de

SUPPORTING INFORMATION

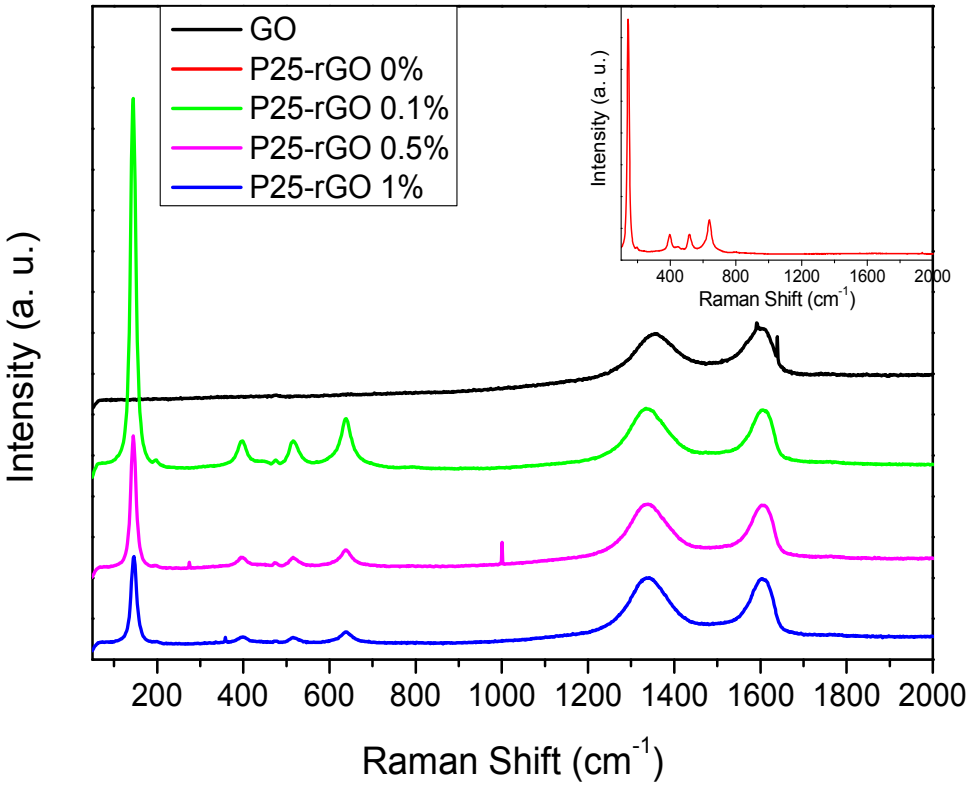

Figure S1. Raman spectra of GO, P25-rGO 0.1%, P25-rGO 0.5%, and P25-rGO 1% normalized to the 1340 cm^{-1} signal; and the magnified spectrum of bare TiO_2 (inset).

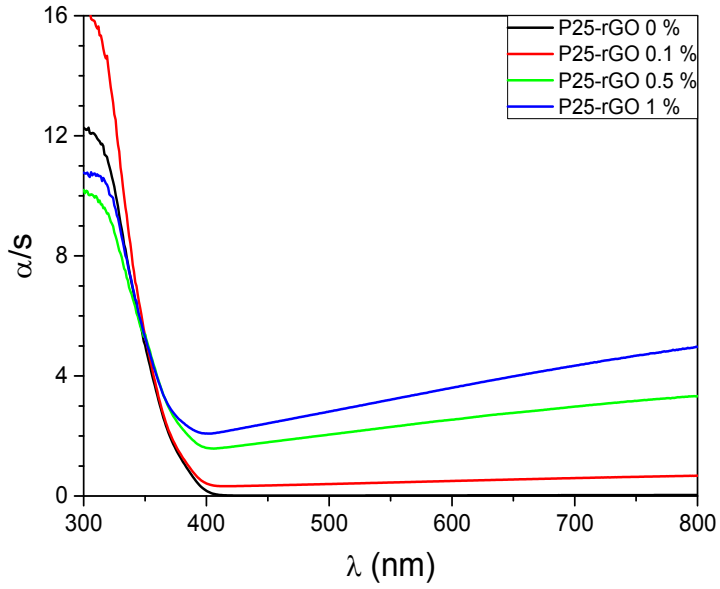

Figure S2. Kubelka-Munk function of the studied P25-rGO nanocomposites.

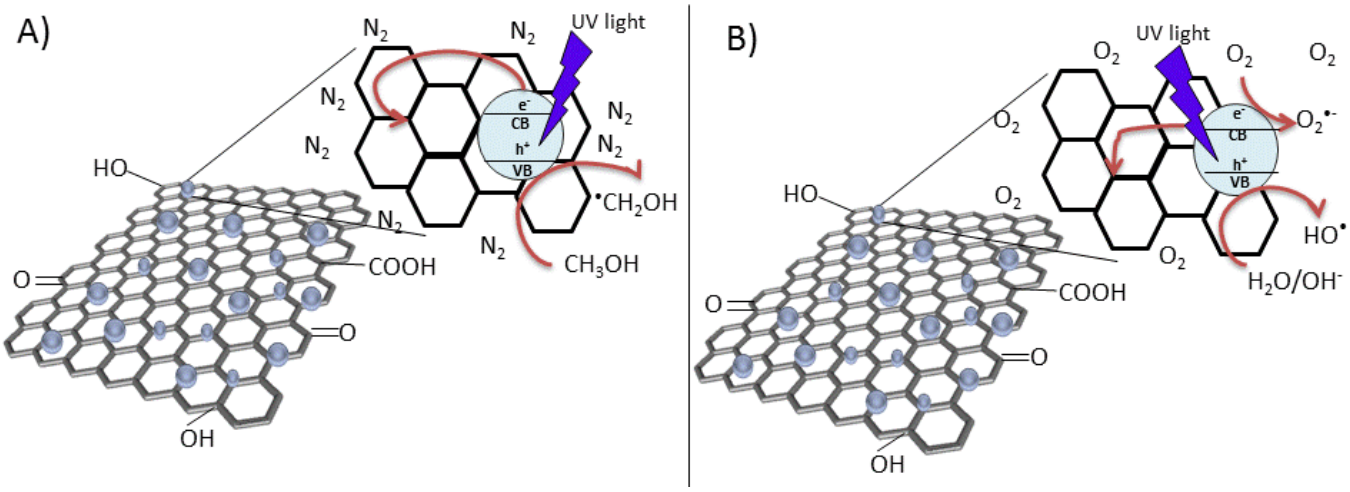

Figure S3. Proposed processes of electron and hole transfer: A) Under N_2 -CH_3OH atmosphere and B) under O_2 atmosphere.

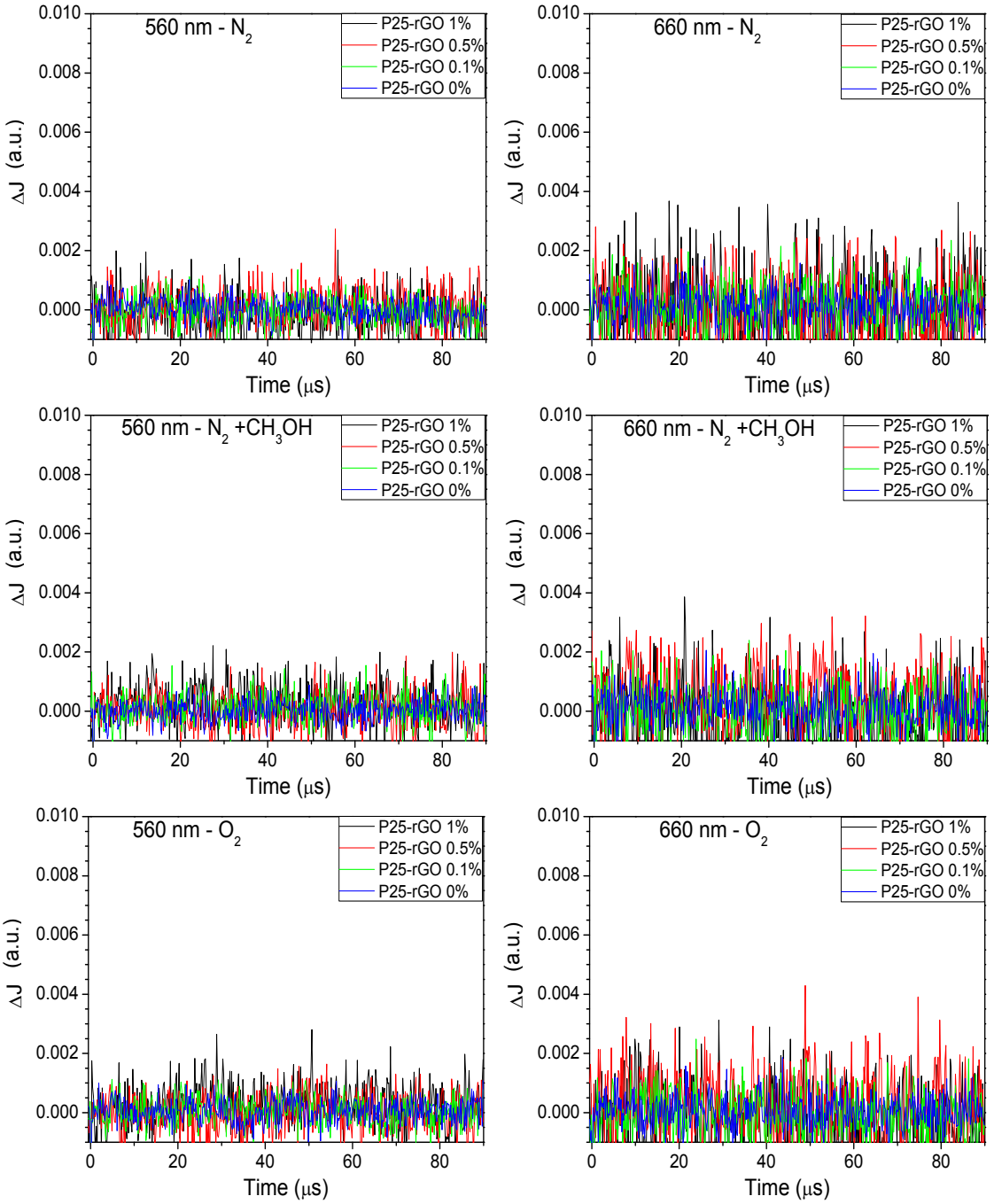

Figure S4. Time profiles of transient absorption at 560 and 660 nm for all the studied nanocomposites with 450 nm excitation (2.1 mJ·cm^{-2}) under N_2, N_2-CH_3OH as hole scavenger and O_2 atmosphere.

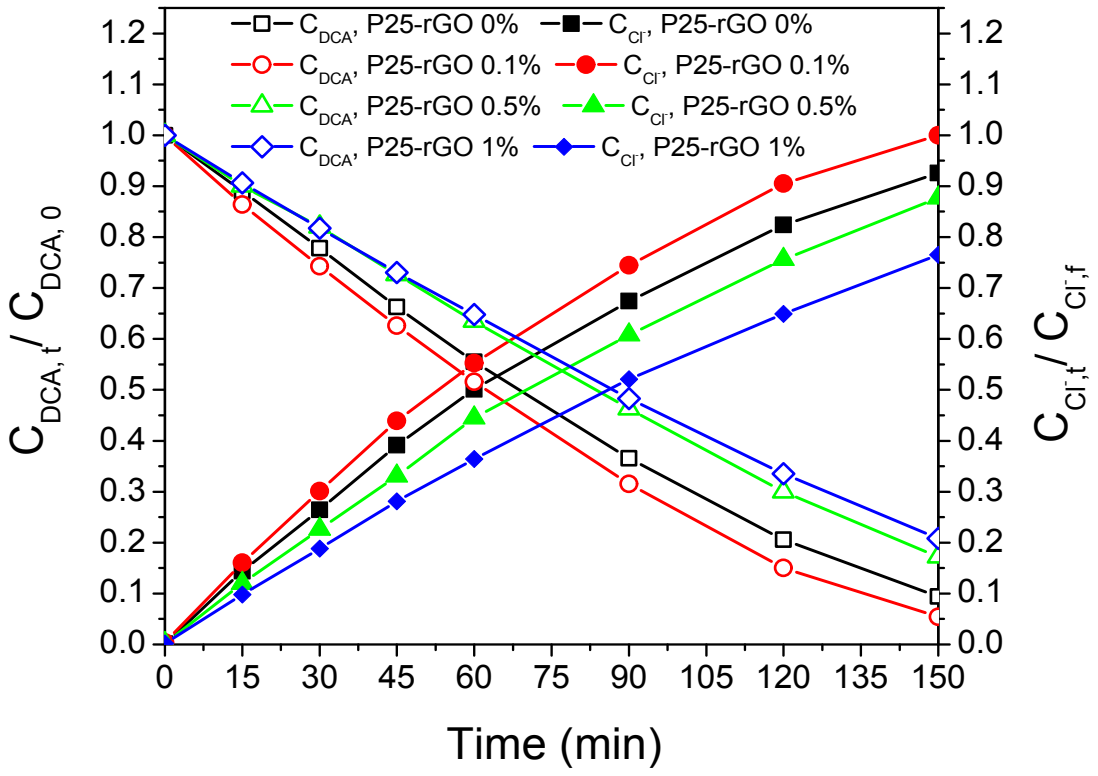

Figure S5. Evolution of the concentration of dichloroacetic acid and chloride formed for the studied P25-rGO nanocomposites.